ACS APPLIED MATERIALS & INTERFACES

www.acsami.org

Research Article

# Conductive Microneedle Patch with Electricity-Triggered Drug Release Performance for Atopic Dermatitis Treatment

Yuan Yang,[▽] Bo Zhi Chen,[▽] Xiao Peng Zhang, Hui Zheng, Zhou Li,* Can Yang Zhang,* and Xin Dong Guo*

Cite This: https://doi.org/10.1021/acsami.2c05952

Read Online

ACCESS | Metrics & More | Article Recommendations | Supporting Information

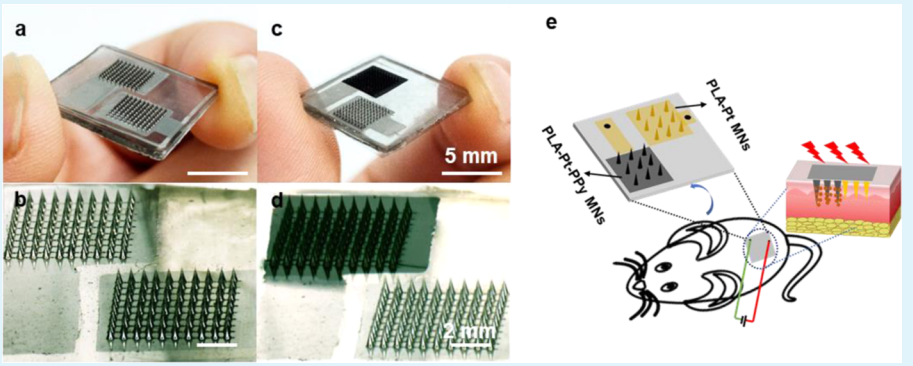


**ABSTRACT:** Atopic dermatitis (AD) is a chronic inflammatory skin disease that seriously affects the life quality of patients. Topical administration of glucocorticoids is considered to be the most effective anti-inflammatory treatment. However, due to the barrier function of skin, only less than 20% of topical drug molecules could diffuse into the skin. Therefore, it is of great importance to develop an effective strategy to improve AD therapy. In this study, we reported a two-electrode microneedle patch (t-EMNP) composed of a polylactic acid−platinum (PLA-Pt) MN array and polylactic acid−platinum−polypyrrole (PLA-Pt-PPy) MN array for improving the transdermal drug delivery efficacy. The drug loading capability of MNs could be altered by employing different polymerization times and drug concentrations. The drug release rate of MNs could be changed by applying different voltages. We further developed a controlled transdermal drug delivery system (c-TDDS) based on this two-electrode microneedle patch (t-EMNP), exhibiting the remarkable performance of the electricity-triggered drug release profile. The drugs could be released with electrical stimulation, while there was almost no drug release without electrical stimulation. For AD treatment *in vivo*, this MN patch with electricity-triggered drug release performance could effectively deliver more drugs into the skin compared with other controls such as dexamethasone cream, which efficiently alleviate AD. In sum, this work not only developed a smart patch for improving AD treatment but also provided a promising approach of transdermal drug delivery on demand.

**KEYWORDS:** *microneedles, electricity-triggered drug release, transdermal drug delivery, two-electrode microneedle patch, atopic dermatitis*



## INTRODUCTION

Atopic dermatitis (AD, often called eczema) is a chronic inflammatory skin disease, from which 15−20% of children and 1−3% of adults are suffering worldwide.[1,2] AD usually presents the symptoms of dry skin, severe erythema, bleeding, edema, and abrasions,[3,4] leading to patient discomfort, sleep deprivation, and diminished self-esteem.[5] Among various treatment options, topical administration of glucocorticoids is widely considered to be the most effective anti-inflammatory treatment.[6,7] However, due to the barrier function of skin, only approximately 10−20% of topical drugs could diffuse into the skin.[8] Moreover, long-term overuse/misuse of this drug may cause serious complications (side effects) such as metabolic disorders, organ injury, and immunosuppression.[5,9] Therefore, it is of great significance to develop a drug delivery system with high drug bioavailability, improved therapeutic efficacy, and reduced side effects.[10,11]

Microneedles (MNs), a novel transdermal drug delivery platform, are minimally invasive devices with the advantages of painless, high patient compliance and high drug delivery efficacy and drug bioavailability,[12−14] which can be used as a useful strategy for AD treatment. In the past decades, various types of MNs such as solid,[15] coated,[16] dissolving,[17,18]

Received: April 7, 2022
Accepted: June 27, 2022

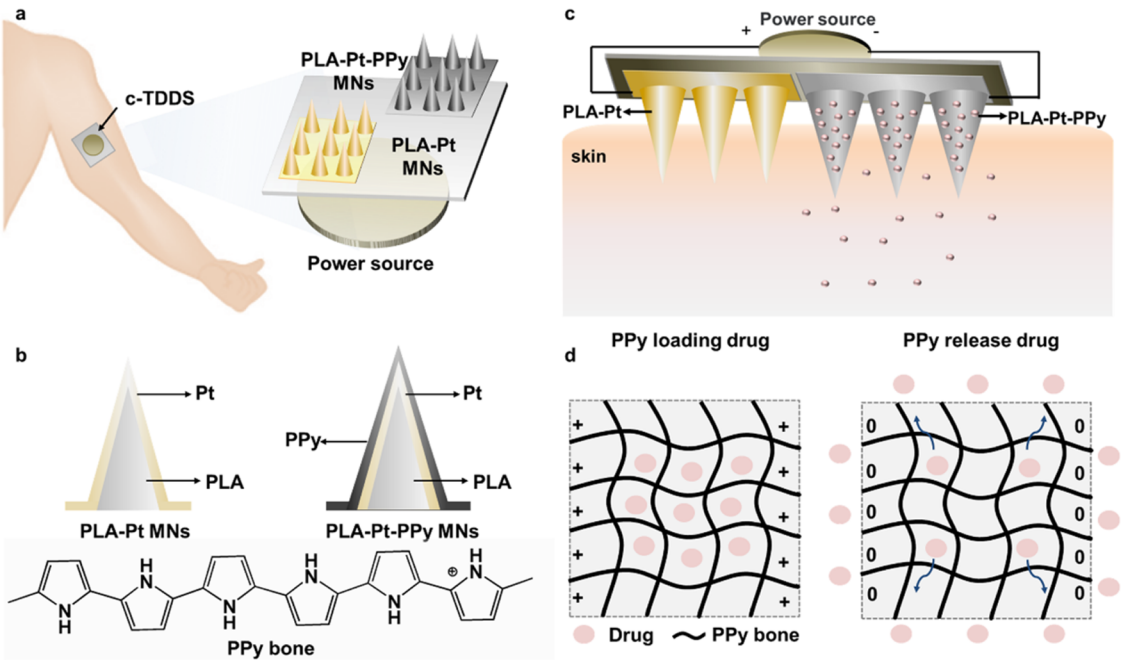


**Figure 1.** Schematic illustration of preparation and drug delivery mechanism of c-TDDS. (a) c-TDDS consisted of a power source, and t-EMNP contained a PLA-Pt MN array and PLA-Pt -PPy MN array. (b) PLA-Pt MNs fabricated by sputtering a layer of Pt on PLA MNs and PLA-Pt-PPy MNs fabricated by depositing a layer of PPy film doping drugs on PLA-Pt MNs. (c) Schematic diagram of drug release form c-TDDS by electrical triggering. (d) Drug release mechanism of c-TDDS.

swellable,[19−21] and hollow MNs[22] have been developed for transdermal drug delivery.[23,24] Generally, the drug molecules enter the skin or the circulation through diffusion from MNs after the MN patch pierced into the skin. However, the drug release performance and spatiotemporal drug concentration are impossible to control at this stage. To meet the special requirements (*e.g.*, controlled release profile) for AD treatment, the controlled drug delivery system based on MNs has attracted more and more attention.[25−28] The system can deliver an appropriate amount of drug to the target site at the appropriate time, which can maintain a stable blood drug concentration, reduce side effects, and improve the drug bioavailability.[29,30] Moreover, the drug release process could be effectively regulated by external stimulation, including light,[31] temperature,[32] magnetism,[33] pH,[34] and electricity.[35] Particularly, electroresponsive MNs facilitated drug delivery by electrical stimulation (ES) based on the mechanism of iontophoresis and electroporation.[35−38] However, it is difficult to achieve precisely controlled release performance in this way. Recently, polypyrrole (PPy), a smart electroresponsive material, can load and release drug molecules by transformation between the oxidative and reductive states, which has been widely investigated and extensively used in biomedical fields.[39,40] It can be used to encapsulate and release anionic,[41,42] cationic,[43] and neutral drugs on demand.[44] For anionic drugs, the principle of encapsulation and release drug of PPy is illustrated in eq 1. The anionic drugs are doped into the PPy bone to neutralize its positive charge, followed by releasing on the reduction of PPy.

$$PPy^{+}/A^{-} \leftrightarrow PPy^{0} + A^{-} \quad (1)$$

In this study, we designed a smart conductive patch based on polylactic acid−platinum−polypyrrole (PLA-Pt-PPy) MNs for improving AD treatment. The drug loading capability and electrotriggered release profile of the MN patch were measured. The drug loading capability of the MN patch was supposed to be regulated by employing the polymerization times and drug concentrations during electrochemical polymerization. The drug could be released by electrical stimulation, while there was almost no drug release without electrical stimulation. To improve AD treatment, we designed an integrative two-electrode microneedle patch (t-EMNP)-based controlled transdermal drug delivery system (c-TDDS), which has the ability to control the drug release profile into the skin of rat by electrical stimulation. The *in vivo* drug delivery mechanism, therapeutic efficacy, and safety of c-TDDS for AD induced by 2,4-dinitrochlorobenzene (DNCB) were carefully studied and evaluated. The electroresponsive conductive MNs could achieve on-demand transdermal drug delivery and an enhanced treatment effect. It would be a promising smart device with excellent drug release performance and good patient compliance for AD and other skin disease treatments.

## RESULTS AND DISCUSSION

**Overview of t-EMNP-Based c-TDDS.** A smart conductive MNP drug delivery system was designed for electrically controlled transdermal release drugs (Figure 1a). The system consisted of a t-EMNP and power source. A t-EMNP contained two MN arrays, drug-loaded PLA-Pt-PPy MN array and PLA-Pt MN array. The PLA-Pt MN array of the t-EMNP was fabricated by sputtering a layer of Pt on PLA MNs. When PPy was oxidized and deposited, the anionic drug could be incorporated into the polymer bone. The drug-loaded PLA-Pt-PPy MN array was fabricated by depositing a layer of PPy film doping drugs on PLA-Pt MNs (Figure 1b). The PLA-Pt MN array and PLA-Pt-PPy MN array were, respectively, connected to the positive and negative electrodes of the power source to form a complete electronically controlled transdermal drug delivery system (c-TDDS). t-EMNP was applied on the skin, and two MN arrays of the t-EMNP and the


https://doi.org/10.1021/acsami.2c05952
ACS Appl. Mater. Interfaces XXXX, XXX, XXX−XXX

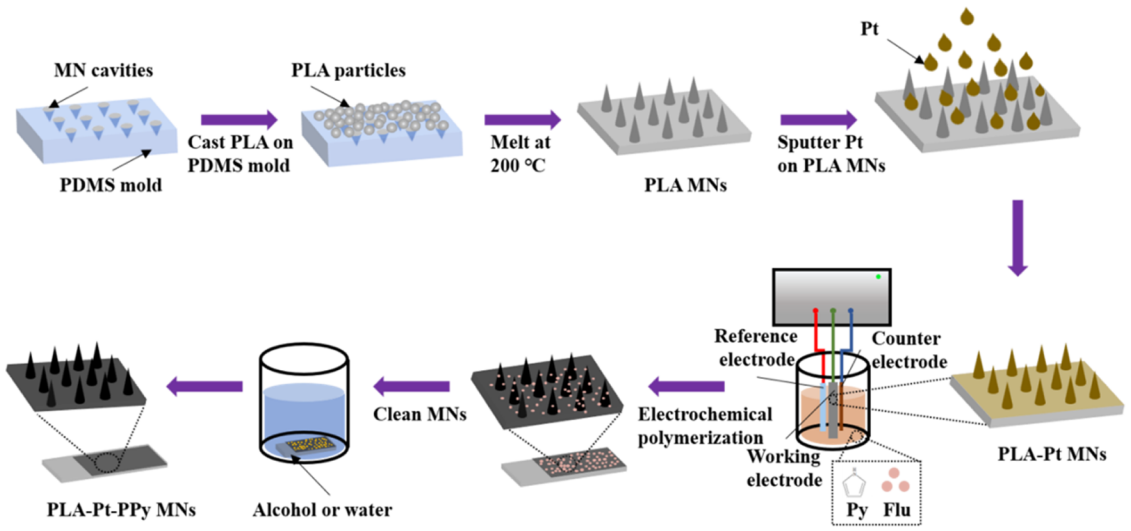


**Figure 2.** Schematic illustration of the fabrication process of PLA-Pt-PPy MNs.

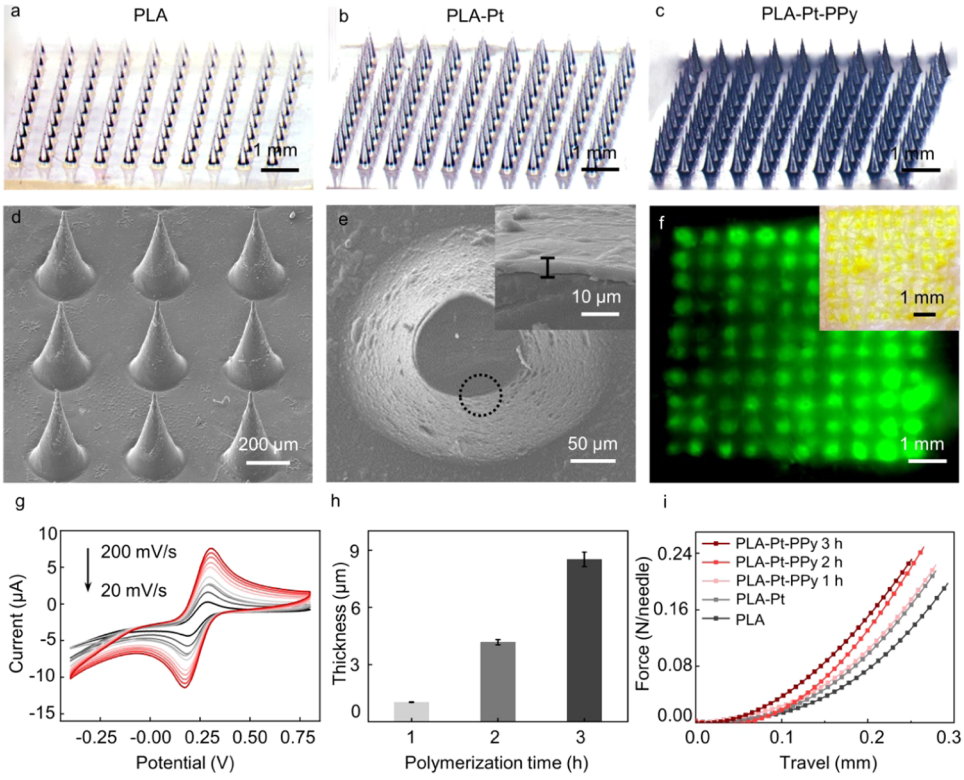


**Figure 3.** Characterization of different MN patches. (a–c) Brightfield micrographs of PLA, PLA-Pt, and PLA-Pt-PPy MNs. (d) SEM image of PLA-Pt-PPy MNs. (e) SEM images of the cross section of PLA-Pt-PPy MNs (inset: the local enlarged view of the cross section of the PLA-Pt-PPy). (f) Images of porcine skin after application of PLA-Pt-PPy MNs under bright and fluorescent field. (g) Cyclic voltammetry (CVs) recorded for the PLA-Pt-PPy MN electrode with the scan rate 20–200 mV/s. (h) Thickness of the PPy/Flu film with the different polymerization times of 1, 2, and 3 h. (i) Force–travel curves of PLA, PLA-Pt, and PLA-Pt-PPy/Flu MNs with the different polymerization times of 1, 2, and 3 h.

external power supply constituted an electrical circuit through the skin tissue interstitial fluid (Figure 1c). In the process of drug release, the PLA-Pt-PPy MN arrays acted as the cathode for the reduction reaction, and the anionic drug could be doped from the PPy bone and released into the skin at a certain voltage (Figure 1d).

**Fabrication of PLA-Pt-PPy MNs.** The fabrication process of the PLA-Pt-PPy MN patch is shown in Figure 2a. First, PLA MNs were prepared with PLA particles based on the thermal micromolding technique. Second, a layer of Pt was sputtered on the PLA MNs to obtain PLA-Pt MNs. Finally, the PLA-Pt MN patch, Pt plate, and saturated calomel electrode (SCE) were used as the working electrode, counter electrode, and reference electrode, respectively, and the anionic model drug, fluorescein sodium (Flu), was used as the dopant, followed by preparing the MN patch through electrochemical deposition of the Flu-doped PPy film on PLA-Pt MNs. After washing with deionized water and drying at room temperature, the PLA-Pt-PPy MN patch was obtained.


https://doi.org/10.1021/acsami.2c05952
ACS Appl. Mater. Interfaces XXXX, XXX, XXX–XXX

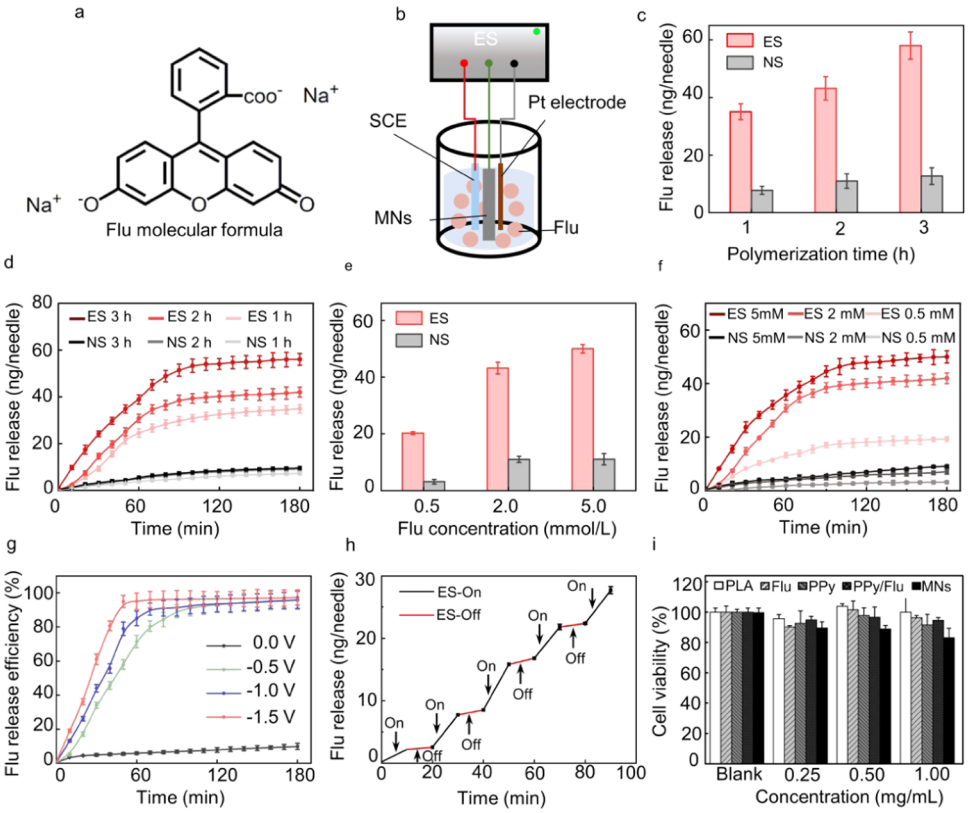


**Figure 4.** Drug delivery mechanism study *in vitro*. (a) Molecular structure of Flu. (b) Schematic diagram of the *in vitro* Flu release process from PLA-Pt-PPy MNs. (c) Amount of Flu in PLA-Pt-PPy MNs at different polymerization times of 1, 2, and 3 h with or without ES. (d) Under ES and NS conditions, Flu cumulative release profiles from PLA-Pt-PPy MNs at different polymerization times of 1, 2, and 3 h. (e) Flu loading of PLA-Pt-PPy MNs at different Flu concentrations of 0.5, 2, and 5 mmol/L. (f) Under ES and NS conditions, Flu cumulative release profiles for PLA-Pt-PPy MNs at different Flu concentrations of 0.5, 2, and 5 mmol/L. (g) Flu release efficiency of PLA-Pt-PPy MNs under different potentials of 0.0, −0.5, −1.5, and −2.0 V. (h) Pulsed release profiles of Flu from PLA-Pt-PPy MNs under −1 V (ES-on for 10 min) and 0 V (ES-off for 10 min). (i) *In vitro* cytotoxicity of PLA, Flu, PPy, PPy, and PLA-Pt-PPy MNs.

**Characterization of the MN Patch.** The PLA MN patch was designed to be a 10 × 10 array on a 6 × 6 mm patch (Figure 3a). A gray layer of Pt was sputtered on the solid PLA MNs to prepare PLA-Pt MNs (Figure 3b). The scanning electron microscopy (SEM) images of PLA MNs and PLA-Pt MNs demonstrated that each MN was conical with a base diameter of 300 $\mu$m and a height of 600 $\mu$m. The surfaces of PLA MNs and PLA-Pt MNs were smooth without any cracks (Figure S1a,b). After a period of electrochemical polymerization for 2 h, the PLA-Pt MN patch was coated with a black layer of PPy film to gain PLA-Pt-PPy MNs (Figure 3c). The resultant PLA-Pt-PPy MNs showed a rough surface, which was a thin film coated on the PLA-Pt shafts (Figure 3d,e). These results indicated that a new conductive MN patch was successfully prepared.

Sufficient mechanical strength is essential for MNs to penetrate the skin. In this work, the mechanical performances of the prepared PLA MNs, PLA-Pt MNs, and PLA-Pt-PPy MNs were measured by inserting them into porcine skin. The yellow dots on the surface of the skin indicated that the microchannels were successfully created by this MN patch, showing that the MN patch achieved almost 100% successful insertions (Figures 3f and S1c). At the same time, by observing the morphology of MNs before and after piercing into the porcine skin, the MN tips did not bend, displaying that these MNs had great mechanical properties (Figure S1a,d).

Next, since the electrochemical performance of the PLA-Pt-PPy MNs was a crucial characterization for drug loading and drug release, cyclic voltammetry (CV) was applied to investigate the charge transfer capacity of the PLA-Pt-PPy MNs. As shown in Figure 3g, its oxidation potential and reduction potential were 0.30 and 0.17 V, respectively, indicating that the potential difference was 0.13 V. The redox peak current tended to be symmetrical, and the peak current value was basically equal. As the scan rate decreased, the half-peak potential decreased weakly, and the potential difference decreased slightly. The redox peak current of MNs had a linear relationship with the square root of the scan rate. The linear relation of oxidation peaks was $y = 0.25339+0.60746x$, $R^2 = 0.99962$, and the linear relation of reduction peak was $y = -0.06486-0.67365x$, $R^2 = 0.99924$ (Figure S2a). Multiple CV scans were used to investigate the stability of the PLA-Pt-PPy MN electrode (Figure S2b). The CV curves of the MNs were almost consistent, which indicated that the MN electrode possessed excellent stability. In addition, as measured by electrochemical impedance spectroscopy (EIS), the equivalent resistance of PLA-Pt-PPy MNs was approximately 11 KΩ with a certain conductivity (Figure S2c).

To investigate the effect of polymerization time on the PLA-Pt-PPy MNs, the MNs were prepared with different electrochemical deposition times of 1, 2, and 3 h. The brightfield image of MNs showed that the tip of PLA-Pt-PPy MNs with 3 h polymerization time was dulled to difficultly penetrate the


https://doi.org/10.1021/acsami.2c05952
ACS Appl. Mater. Interfaces XXXX, XXX, XXX−XXX

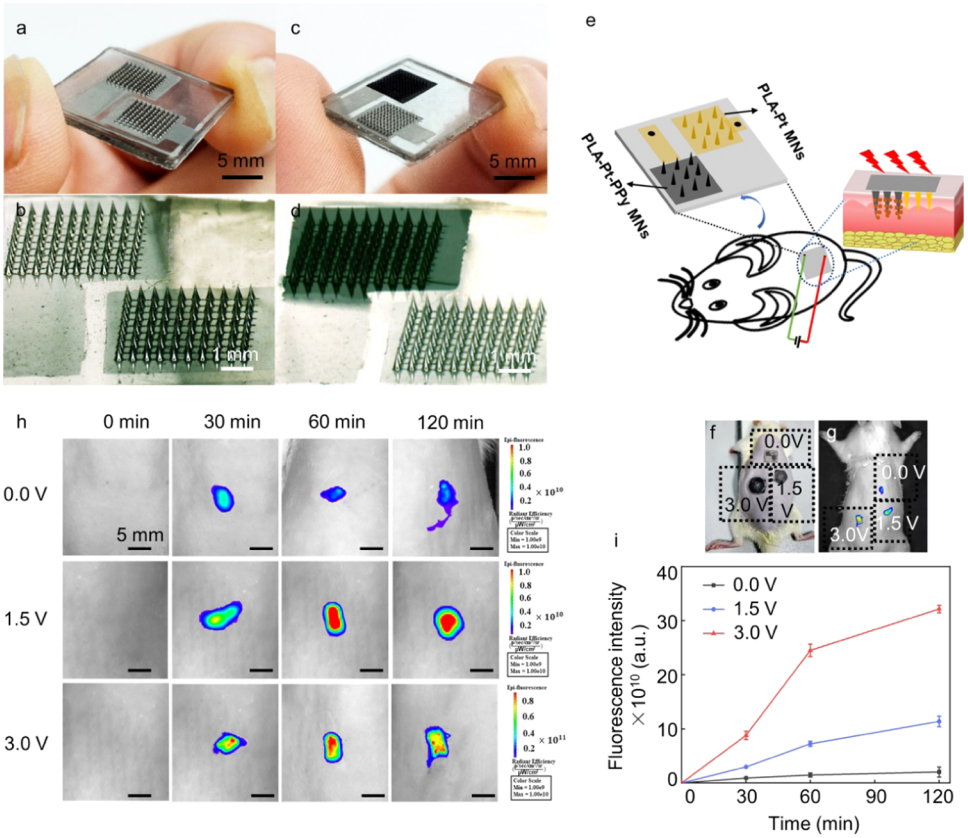


**Figure 5.** *In vivo* drug delivery and release performances study of two-electrode microneedle patch-based transdermal drug delivery. (a, b) PLA-Pt MN patch containing two PLA-Pt MN arrays. (c, d) t-EMNP containing the PLA-Pt-PPy MN array and PLA-Pt MN array. (e) Schematic diagram of the c-TDDS releasing drug in rat. (f) Rat dorsum inserted with three t-EMNP connected to the battery of 0 V (NS), 1.5, and 3.0 V. (g) Fluorescence images of the rat after inserted with three t-EMNP connected to the battery of 0 V (NS), 1.5, and 3.0 V. (h, i) Fluorescence images and fluorescence intensity of the skin site treated with three t-EMNP connected to the battery of 0 V (NS), 1.5, and 3.0 V for 0, 30, 60, and 120 min.

skin (Figure S3). The SEM images displayed that the thicknesses of the PPy film of PLA-Pt-PPy MNs with different polymerization times of 1, 2, and 3 h were 1.032 ± 0.1, 4.612 ± 0.1, and 8.072 ± 0.2 $\mu$m, respectively (Figures S3 and 3h), suggesting that the thickness of the PPy film was increased with the increase of the polymerization time. There was no linear relationship between the polymerization time and film thickness. The reason could be that more oligomers were collected in the electrolyte with the increase of polymerization time, resulting in faster and faster film formation.[45] To confirm whether the PPy film was uniform, the PLA-Pt-PPy MNs with polymerization for 2 h were crosscut at different heights of 600, 500, 350, 250, 150, and 100 $\mu$m. The brightfield images and SEM images showed that the thickness of the PPy film at different heights of MN were almost the same (about 4.7 $\mu$m), which proved that the galvanostatic electrochemical polymerization method could be used to form a homogeneous PPy film on the PLA-Pt MN patch (Figure S4). To further explore the effect of the PPy film on the mechanical properties of the MNs, the PLA MNs, PLA-Pt MNs, and PLA-Pt-PPy MNs with different polymerization times were measured with a dynamometer (Figure 3i). It can be found that the PLA-Pt MNs and PLA-Pt-PPy MNs were firmer than PLA MNs, and the firmness of PLA-Pt-PPy MNs was increased with the increase of the PPy polymerization time according to the change trend of the slope of the force−displacement curves. These results showed that the Pt layer and PPy film could enhance the mechanical performance of PLA MNs. Young's modulus of the PLA, PLA-Pt, and PLA-Pt-PPy MNs were 58.6, 70.4, and 100.8 MPa, respectively, indicating that the gold layer and PPy film can enhance the mechanical performance of PLA MNs (Figure S5). By comparing the morphology of the MNs before and after the mechanical test, it can be found that the MNs only bent without fracturing (Figure S6), which showed that the MN had high elasticity. Taken together, these results proved that the MNs will not leave debris in the subcutaneous tissue after piercing into the skin.

**Drug Delivery Mechanism Study *In Vitro*.** At a certain negative potential, the PPy was reduced, and anionic dopants were released into the solution, as there was a loss of electrostatic attraction between ions and the PPy backbone.[36] The amount of drug release was controlled by the thickness of the PPy film, the value of applied potential, and the time of ES.[46] Flu was used as the anionic model drug to study the electronically controlled release process of PLA-Pt-PPy MNs *in vitro* (Figure 4a). The drug release study was carried out using an electrochemical workstation in an electrochemical cell containing phosphate buffer saline (PBS) solution, using a three-electrode system with the PLA-Pt-PPy MN patch as the working electrode, the platinum wire as the counter electrode, and the SCE electrode as the reference electrode (Figure 4b). The amounts of Flu loaded in PLA-Pt-PPy MNs with polymerization times of 1, 2, and 3 h were measured to be approximately 35.062 ± 2.753, 43.165 ± 4.058, and 58.03501


https://doi.org/10.1021/acsami.2c05952
ACS Appl. Mater. Interfaces XXXX, XXX, XXX−XXX

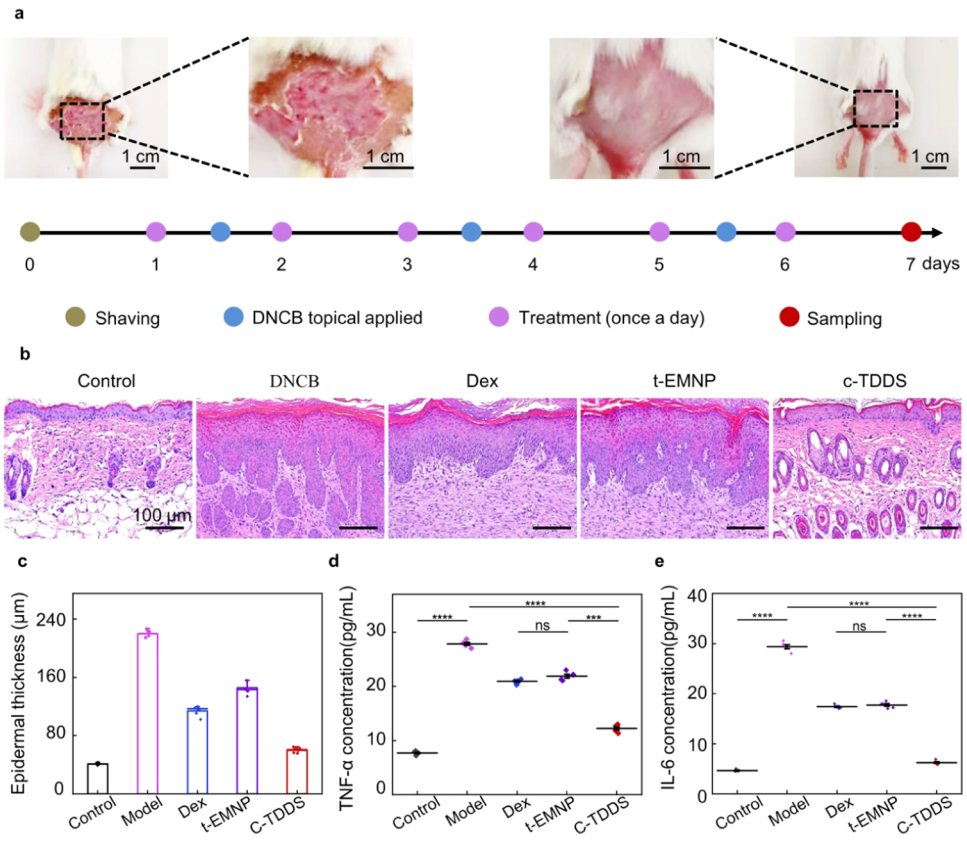


**Figure 6.** Therapeutic efficacy study *in vivo* of c-TDDS for DNCB-induced AD-bearing mice. (a) Timeline and the corresponding photograph of the treatment of DNCB-induced AD-bearing mice. (b) Skin H&E staining images of normal mice, DNCB-induced mice, and DNCB-induced mice treated with Dex solution, t-EMNP, and c-TDDS. (c) Epidermal thicknesses measured in H&E-stained microphotographs. (d, e) Concentration of TNF-$\alpha$ and IL-6 in the skin of normal mice, DNCB-induced mice, and DNCB-induced mice treated with Dex solution, t-EMNP, and c-TDDS.

± 2.09456 ng/needle, respectively (Figure 4c), suggesting that the drug loading capacity of PLA-Pt-PPy MNs increased with the increase of the PPy polymerization time and the thickness of the PPy film. Figure 4d shows the cumulative release of Flu from PLA-Pt-PPy MNs. Under the action of ES, the release rate of Flu was very fast at the beginning, and then, it almost reached equilibrium and attained the maximum cumulative release amount. The maximum cumulative release amounts of Flu from PLA-Pt-PPy with the polymerization times of 1, 2, and 3 h were 34.926 ± 1.846, 41.965 ± 2.098, and 56.035 ± 2.502 ng/needle, respectively. Nevertheless, when there was no stimulation (NS), only a little drug from the surface of PLA-Pt-PPy MNs diffused into the solution (Figure 4d). These results showed that 80−90% of the drug could be released under ES, while only 10−20% of the drug diffused into the PBS solution without ES. Moreover, the longer the electrochemical polymerization time, the thicker the polypyrrole film and the higher the drug loading of PLA-Pt-PPy MNs. However, when the polymerization time was 3 h, the tip of the MN was blunt due to the excessively thick PPy film, making it difficult to penetrate the skin (Figures S3 and S6). Therefore, the polymerization time of 2 h was chosen to prepare PLA-Pt-PPy MNs in the following study.

The electrochemical deposition efficiency of PPy was highly sensitive to the concentration of the anion dopant. The amount of Flu loaded in PLA-Pt-PPy with the Flu concentrations of 0.5, 2, and 5 mmol/L were tested to be about 20.276 ± 0.524, 43.165 ± 2.058, and 49.985 ± 1.499 ng/needle, respectively. (Figure 4e). With ES, the maximum cumulative release amount of Flu from PLA-Pt-PPy with the Flu concentrations 0.5, 2, and 5 mmol/L was 34.926 ± 1.846, 41.965 ± 2.098, and 56.035 ± 2.503 ng/needle, respectively. However, with no ES (NS marked), only a little drug from the surface of PLA-Pt-PPy MNs diffused into the solution (Figure 4f). With the results determined with the certain concentration range of Flu during polymerization, the higher the concentration of the drug, the higher the doping degree of the drug, so the higher the drug loading of the PLA-Pt-PPy/Flu MNs. Therefore, the optimal preparation conditions of PLA-Pt-PPy were electrochemical polymerization for 2 h in 5 mmol/L Flu and 0.1 mol/L Py, considering the abilities of skin insertion and drug loading.

The Flu release efficiency of PLA-Pt-PPy MNs could be regulated by altering the applied voltage (Figure 4g). The efficiency of drug release was higher under −1.5 V because the higher the current output, the more the charges transferred in the circuit and the more the PPy backbone may be in the reduced state at the higher potential, resulting in the release of more drugs. The drug delivery process from PLA-Pt-PPy MNs could be flexibly controlled through on−off of ES (Figure 4h). When ES was on, a linear release profile of Flu was presented, and when ES was off, there was almost no Flu released from the MNs. We further investigated the biocompatibility of the PLA-Pt-PPy by the cytotoxicity test (Figure 4i). The data presented that the cell viability was more than 80% even at the highest concentrations of the material, suggesting that PLA-Pt-PPy MNs had great biocompatibility.


https://doi.org/10.1021/acsami.2c05952
ACS Appl. Mater. Interfaces XXXX, XXX, XXX−XXX

**Microneedle Drug Delivery *In Vivo*.** To facilitate the transdermal administration of the MNs, an integrated two-electrode microneedle patch was fabricated (t-EMNP). A t-EMNP containing two different MN arrays, PLA-Pt-PPy MN array loading Flu and PLA-Pt MN array, was fabricated by depositing PPy on one of the MN arrays of PLA-Pt MNP. Figure 5a,b shows the morphology of the PLA-Pt MNP. There were two identical gray 10 × 10 MN arrays on a 15 × 15 mm patch. The morphology of the t-EMNP is presented in Figure 5c,d. There were two different MN arrays on a patch, of which the gray and black parts (6 mm × 6 mm) were the PLA-Pt MN array and the PLA-Pt-PPy MN array, respectively. To observe the transdermal drug delivery efficiency of t-EMNP, t-EMNP pierced into the porcine skin, and the electrochemical workstation provided a certain voltage. The fluorescence images showed that more Flu was released at the higher potential (Figure S7), indicating that t-EMNP could achieve electrically controllable drug delivery in porcine skin. Next, we designed a portable controlled transdermal drug delivery system (c-TDDS). Using the traditional battery as the power device, two MN arrays were connected to the relevant electrode of the battery (1.5 and 3.0 V) placed in the back of the patch; the PLA-Pt-PPy MN array was connected to the negative electrode of the battery, and the PLA-Pt MN array was connected to the positive electrode of the battery. When the MNs were inserted into the rat skin, the PLA-Pt-PPy MN array and PLA-Pt MN array were connected using skin interstitial fluid to constitute a circuit (Figure 5e). Under 1.5 and 3 V batteries, loop currents were 67 and 131 $\mu$A with good biosafety, respectively (Figure S8a), and the voltages of the PLA-Pt-PPy MN array were 0.87 and 1.23 V due to the existence of the impedance of the skin dermis layer (~10 KΩ) (Figure S8b). The PLA-Pt-PPy MN array as the cathode would facilitate the reduction reaction, and the anionic Flu would break away from the framework of the PPy to achieve drug delivery *in vivo*. The release process of Flu was monitored and imaged using an *in vivo* imaging system (IVIS). Compared with the no electrical stimulation group (0.0 V), there were more than 10 times stronger fluorescent signals in penetration sites with electrical stimulation, and the stronger fluorescent signals were gained at the higher potential. It showed that the Flu could be released from the t-EMNP by ES, and the faster the drug release efficiency with the greater the stimulation voltage, which suggested that the system could achieve electro-responsively controlled drug delivery *in vivo*.

**Therapeutic Efficacy for DNCB-Induced AD *In Vivo*.** To evaluate the application potential of the system in AD treatment, we first constructed a DNCB-induced AD-bearing mouse model on the naked dorsal skin, which showed weight loss and typical lesions, such as skin dryness, severe erythema, hemorrhage, scarring, edema, and excoriation[40] (Figure S9). Then, these AD-bearing mice were selected to be treated with the Dex solution (containing the same content of Dex as t-EMNP), the t-EMNP, and the c-TDDS (t-EMNP connected with a 1.5 V battery). The topical application of the Dex solution was equivalent to the administration mode of the commercial dexamethasone cream. With the treatment of 7 consecutive days, among these various treatments, symptoms of skin edema, bleeding, erythema, abrasion, and erosion were substantially alleviated and the mice's weight gradually returned to normal in the c-TDDS group (Figures 6a and S10). Furthermore, H&E staining showed DNCB-induced AD-bearing mice skin epidermal hyperplasia and inflammatory cell aggregation, and the skin epidermis of AD-bearing mice with the treatment of the system group became obviously thinner, and the inflammatory cell infiltration was significantly decreased, compared with other treatment groups (Figure 6b,c). Meanwhile, the standard ELISA kit results also presented that the concentration of the proinflammatory mediators TNF-$\alpha$ and IL-6 in the skin treated by the c-TDDS was clearly reduced (Figure 6d,e). These results demonstrated that the c-TDDS has a significant therapeutic effect in AD, declaring that t-EMNP with electrical stimulation would release more Dex drugs into the skin. However, Dex solution and t-EMNP without electrical stimulation only had less drugs entering the skin and had no obvious anti-inflammatory effect.

## CONCLUSIONS

In this study, we developed the conductive MNs and t-EMNP for electrically controllable transdermal drug delivery by combining the advantages of the MNs and the PPy film for electrically controlling drug release. These conductive MNs had great mechanical performance, excellent electrochemical property, and high drug loading capability. The t-EMNP-based controlled transdermal drug delivery system (c-TDDS) was able to achieve on-demand release drug by ES and regulate the drug release rate by applying different potentials. The AD-bearing mice treated with c-TDDS could return to normal, and the infiltration of inflammatory cells and inflammatory factors was significantly reduced, suggesting that this conductive MN patch could effectively treat AD disease. We think that this c-TDDS can be used as a versatile device with a high drug loading capacity and electrotriggered drug release profile to effectively deliver one or more anionic drugs, cationic drugs, and neutral drugs for the treatment of many diseases such as arthritis, mental illness, and analgesia. Moreover, this c-TDDS might be modified with some biosensors for detecting biomolecules to form a closed-loop intelligent drug delivery system. When the biosensor converts physiological indicators into electrical signals, the c-TDDS could release drugs on demand. Herein, this study not only developed a smart MN patch for improving AD treatment but also provided a promising platform of on-demand transdermal drug delivery to diagnose and treat different diseases.

## MATERIALS AND METHODS

**Preparation of PLA MNs.** The preparation method of PLA MNs with good biocompatibility and biodegradability was described in our previous work.[47,48] First, a polydimethylsiloxane (PDMS) mold was fabricated using a laser and molding techniques to produce the conical microneedle cavities. Second, PLA particles were placed in the mask of the PDMS mold and heated at 200 °C for 30 min to make the particle melt completely and fill the entire mask. Solid MNs were produced by pressing the melted PLA with a plate and cured at room temperature. Finally, removing the PDMS mold, PLA MNs with a height of 600 $\mu$m and a basal diameter of 300 $\mu$m were successfully prepared.

**Preparation of PLA-Pt -PPy MNs.** PLA-Pt MNs were prepared by spraying a layer of Pt with a thickness of 40 nm on PLA MNs with a sputtering apparatus with 20 mA sputtering current for 30 s and stored in nitrogen. PLA-Pt-PPy MNs loading Flu were prepared using electrochemical deposition in a three-electrode cell, and the PLA-Pt MNs, Pt plate, and saturated calomel electrode (SCE) were used as the working electrode, counter electrode, and reference electrode, respectively. The electrolyte contained 0.1 mol/L Py and 5 mmol/L Flu. The electrochemical deposition was carried out by the constant current density of 0.5 mA/cm$^2$ for 2 h. After preparation, Flu and Py monomers adsorbed on the surface of MNs were washed with alcohol


https://doi.org/10.1021/acsami.2c05952
ACS Appl. Mater. Interfaces XXXX, XXX, XXX−XXX

and deionized water at room temperature and then dried in vacuum. During the preparation process, three different electrochemical deposition durations (1, 2, and 3 h) and three Flu concentrations (0.5, 2, and 5 mmol/L) in electrolytes were used to prepare the PLA-Pt -PPy MNs.

**Characterization of MNs.** A stereomicroscope (SZX7, Olympus, Japan) was used to record the morphology of MNs. A scanning electron microscope (SEM; JSM 6390, JEOL, Tokyo, Japan) was used to observe the morphology of the PLA-Pt -PPy MNs and the thickness of the PPy film.

**Mechanical Performance of MNs.** A dynamometer (Mark-10, Force Gauge Model) was used to measure the mechanical properties of the MNs. In detail, the PLA, PLA-Pt, and PLA-Pt-PPy MN patch were fixed on the platform, and the mechanical sensor moved down to the horizontal platform at a speed of 0.5 mm/min. When the sensor touched the tip of MNs and applied pressure to the MNs, the sensor continually recorded the force and distance traveled. The mechanical properties of the MNs were analyzed according to the force−travel curves. The morphology of the MNs before and after the force measurement was observed with a bright microscope.

**Electrochemical Performance of MNs.** The cyclic voltammetry (CV) method was used to investigate the electrochemical performance of the PLA-Pt-PPy MN electrode, which was carried out in the mixed solution containing 0.1 mol/L KCl and 0.01 mol/L $K_3[Fe(CN)_6]$ deionized water. The Pt plate electrode and SCE were utilized as the counter electrode and reference electrode, respectively.

**Measurement of the Drug Loading and Drug Delivery Efficiency.** The electrically stimulated Flu release from the PLA-Pt-PPy MNs with different polymerization times and different Flu concentrations was tested in a three-electrode cell. The working electrode, counter electrode, and reference electrode were the PLA-Pt -PPy MNs, Pt plate, and SCE, respectively. The electrolyte was 1.5 mL of PBS PH (7.2−7.4) stirred with a magnetic bar at room temperature. The drug loading of PLA-Pt-PPy MNs was determined by applying a constant potential of −1.0 V for 24 h. The Flu cumulative release process was tested for 2 h under −1.0 V, and the electrolyte was collected and replaced with fresh PBS every 10 min. Three different ES potentials (−0.5, −1.0, and −1.5 V) were applied to investigate the effect of the ES potential on the efficiency of Flu release. Pulse potentials (0.0 V for 10 min and −1.0 V for 10 min) were used to characterize the on-demand drug delivery profile of PLA-Pt-PPy MNs. The Flu concentration was measured using a microplate reader (Fluoroskan Ascent, Thermo Scientific, China).

**Cytotoxicity of PLA-Pt-PPy MNs.** The cytotoxicity of PLA-Pt-PPy MNs was evaluated against mouse fibroblast cell lines (L-929 cells) using a CCK-8 array. L-929 cells were cultured in Dulbecco's modified Eagle medium (DMEM) containing 10% fetal bovine serum (FBS) and 1% penicillin−streptomycin (PS) and incubated in a humidified incubator (37 °C, 5% $CO_2$). The absorbance of each simple was tested at 450 nm with a microplate reader (EnSpire, PerkinElmer, MA).

**Preparation of t-EMNP.** t-EMNP contained two different MN arrays, PLA-Pt MN array and PLA-Pt-PPy MN array, which was prepared through the following three steps. First, PLA MNP containing two 10 × 10 MN arrays were fabricated by a high-temperature thermoforming process based on the designed PDMS mold. Second, the PLA MNP was covered with some mask and sputtered with a layer of Pt. A MNP containing two PLA-Pt MN arrays was obtained after removing the mask. Finally, one of the two PLA-Pt MN arrays was regarded as the working electrode, and the Pt plate and SCE were used as the counter electrode and reference electrode, respectively. The electrolyte contained 0.1 mol/L Py and 5 mmol/L Flu or Dex. The PPy film loading the drug was deposited on the working electrode by a constant current density of 0.5 mA/cm$^2$ for 2 h. There were two different MN arrays, PLA-Pt MN array and PLA-Pt-PPy on a patch, which was defined as t-EMNP. The Flu (model drug)-loaded t-EMNP was used to explore the drug release kinetics of the system *in vivo*, and Dex-loaded t-EMNP was used to treat AD *in vivo*. Since Dex and Flu had similar molecular structures, under the same preparation conditions, the drug loading contents in t-EMNP were almost similar.

**Drug Delivery *In Vitro* and *In Vivo*.** t-EMNP was applied on the porcine cadaver skin, and then, two MN arrays, the working electrode PLA-Pt-PPy MN array and the counter electrode PLA-Pt MN array, were connected to the corresponding electrode wires of the electrochemical workstation, which provided different stimulation voltages of 0.0 V (NS), −1.5, and −3.0 V. After stimulating for 1 h, the t-EMNP was removed, and the section of the skin was imaged under a fluorescence microscope to determine the drug delivery efficiency in porcine skin.

Female Sprague−Dawley (SD) rats (200 ± 10 g) were used to measure the drug delivery efficiency of t-EMNP in vivo. Using a traditional battery as the power source, the working electrode PLA-Pt-PPy MNs and the counter electrode PLA-Pt MN on the t-EMNP were, respectively, connected to the positive and negative electrodes of the battery. The PLA-Pt-PPy MN array was connected to the negative electrode, and the PLA-Pt MN array was connected to the positive electrode. The battery was attached to the back of the MN patch to obtain an integrated electrically controlled drug delivery system (c-TDDS). The system penetrated the skin of the rats to form a complete electrical circuit and remained embedded for different times of 0, 30, 60, and 120 min with batteries of different voltages, 0.0 V (no battery), 1.5, and 3.0 V. Next, the rats were imaged using an *in vivo* imaging system (IVIS, Xenogen 200, Caliper Life Sciences, Hopkinton, MA) to measure the fluorescent intensity of Flu and decide the drug delivery efficiency *in vivo*.

**Evaluation of Therapeutic Efficacy for AD *In Vivo*.** For preparation of the AD mice model, after the dorsal hair was removed, 25 male BALB/c mice (6−8 weeks) were randomly divided into 5 groups (health control group, AD model group, Dex-treated group, t-EMNP-treated group, and c-TDDS-treated group). DNCB dissolved in a 2:1 mixture of acetone/olive oil was used to induce AD in the mice except for the control group. The delimited area of the back skin (2 × 2) was stimulated with 100 μL of 1% DNCB every day for one week. Then, 100 μL of 0.5% DNCB was repeatedly applied to the skin once every two days for two consecutive weeks.

For treatment of AD-bearing mice, the mice in the Dex group, the t-EMNP group, and the c-TDDS group were treated with Dex solution (100 μL, 0.5 mg/mL), t-EMNP (no electrical stimulation), and c-TDDS (t-EMNP connected with a 1.5 V battery) for 1 h every day, respectively. After 7 days, the mice were sacrificed to collect the skin tissue. The skin tissue samples were stained with hematoxylin and eosin (H&E) to observe the skin appearance and inflammation infiltration. The inflammatory factors of TNF-α and IL-6 in the skin were measured using a using standard ELISA kit.

## ■ ASSOCIATED CONTENT

### Supporting Information

The Supporting Information is available free of charge at https://pubs.acs.org/doi/10.1021/acsami.2c05952.

Brightfield and SEM images of MNs, images of porcine skin after application of MNs under bright and fluorescent fields, CVs and EIS curves of PLA-Pt-PPy MNs, thickness of the PPy film including different polymerization times and different MN heights, Young's modulus of MN, brightfield images of MNs before and after mechanical testing, fluorescent field images of the porcine skin after application of MNP applied different voltage ES, current in the circuit and voltage loaded on the PLA-Pt-PPy MN array penetrating the skin from 1.5 and 3.0 V batteries, body weight of DNCB-induced AD-bearing mice, and body weight of AD-bearing mice with different treatments (PDF)



https://doi.org/10.1021/acsami.2c05952
ACS Appl. Mater. Interfaces XXXX, XXX, XXX−XXX

## AUTHOR INFORMATION


### Corresponding Authors

**Zhou Li** − *CAS Center for Excellence in Nanoscience Beijing Key Laboratory of Micro-nano Energy and Sensor, Beijing Institute of Nanoenergy and Nanosystems, Chinese Academy of Sciences, Beijing 101400, China; School of Nanoscience and Technology, University of Chinese Academy of Sciences, Beijing 100049, China; Center of Nanoenergy Research School of Physical Science and Technology, Guangxi University, Nanning 530004, China;* orcid.org/0000-0002-9952-7296; Email: zli@binn.cas.cn

**Can Yang Zhang** − *Institute of Biopharmaceutical and Health Engineering, Shenzhen International Graduate School, Tsinghua University, Shenzhen 518055, China;* orcid.org/0000-0002-6975-5781; Email: zhang.cy@sz.tsinghua.edu.cn

**Xin Dong Guo** − *Beijing Laboratory of Biomedical Materials, College of Materials Science and Engineering, Beijing University of Chemical Technology, Beijing 100029, China;* orcid.org/0000-0001-5581-4253; Email: xdguo@buct.edu.cn

### Authors

**Yuan Yang** − *Beijing Laboratory of Biomedical Materials, College of Materials Science and Engineering, Beijing University of Chemical Technology, Beijing 100029, China; CAS Center for Excellence in Nanoscience Beijing Key Laboratory of Micro-nano Energy and Sensor, Beijing Institute of Nanoenergy and Nanosystems, Chinese Academy of Sciences, Beijing 101400, China; School of Nanoscience and Technology, University of Chinese Academy of Sciences, Beijing 100049, China*

**Bo Zhi Chen** − *Beijing Laboratory of Biomedical Materials, College of Materials Science and Engineering, Beijing University of Chemical Technology, Beijing 100029, China;* orcid.org/0000-0001-5784-3314

**Xiao Peng Zhang** − *Beijing Laboratory of Biomedical Materials, College of Materials Science and Engineering, Beijing University of Chemical Technology, Beijing 100029, China; Institute of Biopharmaceutical and Health Engineering, Shenzhen International Graduate School, Tsinghua University, Shenzhen 518055, China*

**Hui Zheng** − *Department of Anesthesiology, National Cancer Center/National Clinical Research Center for Cancer/Cancer Hospital, Chinese Academy of Medical Sciences and Peking Union Medical College, Beijing 100021, China*

Complete contact information is available at: https://pubs.acs.org/10.1021/acsami.2c05952

### Author Contributions

[▽]Y.Y. and B.Z.C. contributed equally to this paper.


### Notes

The authors declare no competing financial interest.

## ACKNOWLEDGMENTS

This work was financially supported by the National Natural Science Foundation of China (51873015 and 51673019) and the long-term subsidy mechanism from the Ministry of Finance and the Ministry of Education of PRC, Start-up package at Institute of Biopharmaceutical and Health Engineering at Tsinghua University (01010600002). The authors thank everyone who contributed to this work and also the references for their comments.

## REFERENCES


(1) Yin, J.; Yoon, S. H.; Ahn, H. S.; Lee, M. W. Inhibitory Activity of Allergic Contact Dermatitis and Atopic Dermatitis-Like Skin in BALB/c Mouse through Oral Administration of Fermented Barks of Alnus sibirica. *Molecules* **2018**, *23*, 450−462.

(2) Feng, J.; Yang, P.; Mack, M. R.; Dryn, D.; Luo, J. L.; Gong, X.; Liu, S. B.; Oetjen, L. K.; Zholos, A. V.; Mei, Z.; Yin, S. J.; Kim, B. S.; Hu, H. Z. Sensory TRP Channels Contribute Differentially to Skin Inflammation and Persistent Itch. *Nat. Commun.* **2017**, *8*, No. 980.

(3) Choi, D. W.; Kwon, D. A.; Jung, S. K.; See, H. J.; Jung, S. Y.; Shon, D. H.; Shin, H. S. Silkworm Dropping Extract Ameliorate Trimellitic Anhydride-Induced Allergic Contact Dermatitis by Regulating Th1/Th2 Immune Response. *Biosci., Biotechnol., Biochem.* **2018**, *82*, 1531−1538.

(4) Shi, H. J.; Song, H. B.; Gao, Q.; Si, J. W.; Zou, Q. Combination of Oxymatrine and Diammonium Glycyrrhizinate Significantly Mitigates Mice Allergic Contact Dermatitis Induced by Dinitrofluorobenzene. *Exp. Biol. Med.* **2019**, *244*, 1111−1119.

(5) Weidinger, S.; Beck, L. A.; Bieber, T.; Kabashima, K.; Irvine, A. D. Atopic dermatitis. *Nat. Rev. Dis. Primers* **2018**, *4*, No. 1.

(6) Welsch, K.; Holstein, J.; Laurence, A.; Ghoreschi, K. Targeting JAK/STAT Signalling in Inflammatory Skin Diseases with Small Molecule Inhibitors. *Eur. J. Immunol.* **2017**, *47*, 1096−1107.

(7) Tang, W.; Yang, J. B.; Zhao, Z. B.; Lian, Z. X.; Liang, G. L. Intracellular Coassembly Boosts the Anti-inflammation Capacity of Dexamethasone. *Nanoscale* **2017**, *9*, 17717−17721.

(8) Prausnitz, M. R.; Langer, R. Transdermal Drug Delivery. *Nat. Biotechnol.* **2008**, *26*, 1261−1268.

(9) Zhang, R. J.; Liu, R. F.; Liu, C.; Pan, L. N.; Qi, Y. T.; Cheng, J.; Guo, J. W.; Jia, Y.; Ding, J.; Zhang, J. X.; Hu, H. Y. A pH/ROS Dual-Responsive and Targeting Nanotherapy for Vascular Inflammatory Diseases. *Biomaterials* **2020**, *230*, No. 119605.

(10) Wan, T.; Pan, Q.; Ping, Y. Microneedle-Assisted Genome Editing: A Transdermal Strategy of Targeting NLRP3 by CRISPR-Cas9 for Synergistic Therapy of Inflammatory Skin Disorders. *Sci. Adv.* **2021**, *7*, No. eabe2888.

(11) Jang, M. Y.; Kang, B. M.; Yang, H.; Ohn, J.; Kwon, O.; Jung, H. High-Dose Steroid Dissolving Microneedle for Relieving Atopic Dermatitis. *Adv. Healthcare Mater.* **2021**, *10*, No. 2001691.

(12) Zhang, X. X.; Fu, X.; Chen, G. P.; Wang, Y. T.; Zhao, Y. J. Versatile Ice Microneedles for Transdermal Delivery of Diverse Actives. *Adv. Sci.* **2021**, *8*, No. 2101210.

(13) Zhang, Y. Q.; Yu, J. C.; Kahkoska, A. R.; Wang, J. Q.; Buse, J. B.; Gu, Z. Advances in Transdermal Insulin Delivery. *Adv. Drug Delivery Rev.* **2019**, *139*, 51−70.

(14) Wang, F. Y.; Zhang, X. X.; Chen, G. P.; Zhao, Y. J. Living Bacterial Microneedles for Fungal Infection Treatment. *Research* **2020**, *2020*, 1−9.

(15) Li, Q. Y.; Zhang, J. N.; Chen, B. Z.; Wang, Q. L.; Guo, X. D. A Solid Polymer Microneedle Patch Pretreatment Enhances the Permeation of Drug Molecules into the Skin. *RSC Adv.* **2017**, *7*, 15408−15415.

(16) Chen, Y.; Chen, B. Z.; Wang, Q. L.; Jin, X.; Guo, X. D. Fabrication of Coated Polymer Microneedles for Transdermal Drug Delivery. *J. Controlled Release* **2017**, *265*, 14−21.

(17) Du, H. Y.; Liu, P.; Zhu, J. J.; Lan, J. J.; Li, Y.; Zhang, L. B.; Zhu, J. T.; Tao, J. Hyaluronic Acid-Based Dissolving Microneedle Patch Loaded with Methotrexate for Improved Treatment of Psoriasis. *ACS Appl. Mater. Interfaces* **2019**, *11*, 43588−43598.

(18) Ye, Y. Q.; Wang, C.; Zhang, X. D.; Hu, Q. Y.; Zhang, Y. Q.; Liu, Q.; Wen, D.; Milligan, J. S.; Bellotti, A.; Huang, L.; Dotti, G.; Gu, Z. A Melanin-Mediated Cancer Immunotherapy Patch. *Sci. Immunol.* **2017**, *2*, No. eaan5692.

(19) Qu, M.; Kim, H.-J.; Zhou, X. W.; Wang, C.; Jiang, X. R.; Zhu, J. X.; Xue, Y. M.; Tebon, P.; Sarabi, S. A.; Ahadian, S.; Dokmeci, M. R.; Zhu, S. S.; Gu, Z.; Sun, W. J.; Khademhosseini, A. Biodegradable

Microneedle Patch for Transdermal Gene Delivery. *Nanoscale* **2020**, *12*, 16724−16729.
(20) Chen, B. Z.; Zhang, L. Q.; Xia, Y. Y.; Zhang, X. P.; Guo, X. D. A Basal-bolus Insulin Regimen Integrated Microneedle Patch for Intraday Postprandial Glucose Control. *Sci. Adv.* **2020**, *6*, No. eaba7260.
(21) Yang, S. Y.; O'Cearbhaill, E. D.; Sisk, G. C.; Park, K. M.; Cho, W. K.; Villiger, M.; Bouma, B. E.; Pomahac, B.; Karp, J. M. A Bio-inspired Swellable Microneedle Adhesive for Mechanical Interlocking with Tissue. *Nat. Commun.* **2013**, *4*, No. 1702.
(22) He, G.; Yang, C. D.; Hang, T.; Liu, D.; Chen, H.-J.; Zhang, A.-H.; Lin, D.; Wu, J. M.; Yang, B.-R.; Xie, X. Hollow Nanoneedle-Electroporation System To Extract Intracellular Protein Repetitively and Nondestructively. *ACS Sens.* **2018**, *3*, 1675−1682.
(23) Kim, Y. C.; Park, J. H.; Prausnitz, M. R. Microneedles for Drug and Vaccine Delivery. *Adv. Drug Delivery Rev.* **2012**, *64*, 1547−1568.
(24) Jamaledin, R.; Yiu, C. K. Y.; Zare, E. N.; Niu, L.-N.; Vecchione, R.; Chen, G. J.; Gu, Z.; Tay, F. R.; Makvandi, P. Advances in Antimicrobial Microneedle Patches for Combating Infections. *Adv. Mater.* **2020**, *32*, No. 2002129.
(25) Gao, B. B.; Guo, M. Z.; Lyu, K.; Chu, T. S.; He, B. F. Intelligent Silk Fibroin Based Microneedle Dressing (i-SMD). *Adv. Funct. Mater.* **2021**, *31*, 2006839.
(26) Yu, J. C.; Wang, J. Q.; Zhang, Y. Q.; Chen, G. J.; Mao, W. W.; Ye, Y. Q.; Kahkoska, A. R.; Buse, J. B.; Langer, R.; Gu, Z. Glucose-responsive Insulin Patch for the Regulation of Blood Glucose in Mice and Minipigs. *Nat. Biomed. Eng.* **2020**, *4*, 499−506.
(27) Wang, J. Q.; Yu, J. C.; Zhang, Y. Q.; Zhang, X. D.; Kahkoska, A. R.; Chen, G. J.; Wang, Z. J.; Sun, W. J.; Cai, L. L.; Chen, Z. W.; Qian, C. G.; Shen, Q. D.; Khademhosseini, A.; Buse, J. B.; Gu, Z. Charge-switchable Polymeric Complex for Glucose-responsive Insulin Delivery in Mice and Pigs. *Sci. Adv.* **2019**, *5*, No. eaaw4357.
(28) Chang, H.; Zheng, M. J.; Chew, S. W. T.; Xu, C. Advances in the Formulations of Microneedles for Manifold Biomedical Applications. *Adv. Mater. Technol.* **2020**, *5*, No. 1900552.
(29) Xu, L. L.; Yang, Y.; Mao, Y. K.; Li, Z. Self-powerbility in Electrical Stimulation Drug Delivery System. *Adv. Mater.Technol.* **2022**, *7*, No. 2100055.
(30) Yang, Y.; Xu, L. L.; Jiang, D. J.; Chen, B. Z.; Luo, R. Z.; Liu, Z.; Qu, X. C.; Wang, C.; Shan, Y. Z.; Cui, Y.; Zheng, H.; Wang, Z. W.; Wang, Z. L.; Guo, X. D.; Li, Z. Self-powered Controllable Transdermal Drug Delivery System. *Adv. Funct. Mater.* **2021**, *31*, No. 2104092.
(31) Hao, Y.; Dong, M. L.; Zhang, T. Y.; Peng, J. R.; Jia, Y. P.; Cao, Y. P.; Qian, Z. Y. Novel Approach of Using Near-Infrared Responsive PEGylated Gold Nanorod Coated Poly(l-Lactide) Microneedles to Enhance the Antitumor Efficiency of Docetaxel-Loaded MPEG-PDLLA Micelles for Treating an A431 Tumor. *ACS Appl. Mater. Interfaces* **2017**, *9*, 15317−15327.
(32) Chen, S. Y.; Miyazaki, T.; Itoh, M.; Matsumoto, H.; Morooka, Y.; Tanaka, M.; Miyahara, Y.; Suganami, T.; Matsumoto, A. Temperature-Stable Boronate Gel-Based Microneedle Technology for Self-Regulated Insulin Delivery. *ACS Appl. Polym. Mater.* **2020**, *2*, 2781−2790.
(33) Zhang, X. X.; Chen, G. P.; Fu, X.; Wang, Y. T.; Zhao, Y. J. Magneto-Responsive Microneedle Robots for Intestinal Macromolecule Delivery. *Adv. Mater.* **2021**, *33*, No. 2104932.
(34) Zhang, Y. Q.; Wang, J. Q.; Yu, J. C.; Wen, D.; Kahkoska, A. R.; Lu, Y.; Zhang, X. D.; Buse, J. B.; Gu, Z. Bioresponsive Microneedles with a Sheath Structure for $H_2O_2$ and pH Cascade-Triggered Insulin Delivery. *Small* **2018**, *14*, No. 1704181.
(35) Kusama, S.; Sato, K.; Matsui, Y.; Kimura, N.; Abe, H.; Yoshida, S.; Nishizawa, M. Transdermal Electroosmotic Flow Generated by A Porous Microneedle Array Patch. *Nat. Commun.* **2021**, *12*, No. 658.
(36) Yang, J. B.; Li, Y. J.; Ye, R.; Zheng, Y.; Li, X. L.; Chen, Y. Z.; Xie, X.; Jiang, L. L. Smartphone-powered Iontophoresis-microneedle Array Patch for Controlled Transdermal Delivery. *Microsyst. Nanoeng.* **2020**, *6*, No. 112.
(37) Wei, Z. W.; Zheng, S. Q.; Wang, R. X.; Bu, X. L.; Ma, H. L.; Wu, Y. D.; Zhu, L.; Hu, Z. Y.; Liang, Z. C.; Li, Z. H. A Flexible Microneedle Array as Low-voltage Electroporation Electrodes for in vivo DNA and siRNA Delivery. *Lab Chip* **2014**, *14*, 4093−4102.
(38) Xia, D. N.; Jin, R.; Byagathvallia, G.; Yue, H.; Ye, L.; Lu, C. Y.; Bhamla, M. S.; Yang, C. L.; Prausnitza, M. R. An Ultra-low-cost Electroporator with Microneedle Electrodes (ePatch) for SARS-CoV-2 Vaccination. *Proc. Natl. Acad. Sci. U.S.A.* **2021**, *118*, No. e2110817118.
(39) Puiggalí-Jou, A.; del Valle, L. J.; Aleman, C. Drug Delivery Systems Based on Intrinsically Conducting Polymers. *J. Controlled Release* **2019**, *309*, 244−264.
(40) Bansal, M.; Dravid, A.; Aqrawe, Z.; Montgomery, J.; Wu, Z.; Svirskis, D. Conducting Polymer Hdrogels for Electrically Responsive Drug Delivery. *J. Controlled Release* **2020**, *328*, 192−209.
(41) Du, Z. J.; Bi, G.-Q.; Cui, X. T. Electrically Controlled Neurochemical Release from Dual-Layer Conducting Polymer Films for Precise Modulation of Neural Network Activity in Rat Barrel Cortex. *Adv. Funct. Mater.* **2018**, *28*, No. 1703988.
(42) Ouyang, Q. L.; Feng, X. L.; Kuang, S. Y.; Panwar, N.; Song, P. Y.; Yang, C. B.; Yang, G.; Hemu, X. Y.; Zhang, G.; Yoon, H. S.; Tam, J. P.; Liedberg, B.; Zhu, G.; Yong, K.-T.; Wang, Z. L. Self-Powered, On-Demand Transdermal Drug Delivery System Driven by Triboelectric Nanogenerator. *Nano Energy* **2019**, *62*, 610−619.
(43) Hosseini-Nassab, N.; Samanta, D.; Abdolazimi, Y.; Annes, J. P.; Zare, R. N. Electrically Controlled Release of Insulin Using Polypyrrole Nanoparticles. *Nanoscale* **2017**, *9*, 143−149.
(44) Samanta, D.; Hosseini-Nassab, N.; McCarty, A. D.; Zare, R. N. Ultra-low Voltage Triggered Release of An Anticancer Drug from Polypyrrole Nanoparticles. *Nanoscale* **2018**, *10*, 9773−9779.
(45) Krukiewicz, K.; Zawisza, P.; Herman, A. P.; Turczyn, R.; Boncel, S.; Zak, J. K. An Electrically Controlled Drug Delivery System Based on Conducting poly(3,4-ethylenedioxypyrrole) Matrix. *Bioelectrochemistry* **2016**, *108*, 13−20.
(46) Ge, D. T.; Tian, X. D.; Qi, R. C.; Huang, S. Q.; Mu, J.; Hong, S. M.; Ye, S. F.; Zhang, X. M.; Li, D. H.; Shi, W. A Polypyrrole-based Microchip for Controlled Drug Release. *Electrochim. Acta* **2009**, *55*, 271−275.
(47) Wang, Q. L.; Zhu, D. D.; Chen, Y.; Guo, X. D. A Fabrication Method of Microneedle Molds with Controlled Microstructures. *Mater. Sci. Eng., C* **2016**, *65*, 135−142.
(48) DeStefano, V.; Khan, S.; Tabada, A. Applications of PLA in Modern Medicine. *Eng. Regener.* **2020**, *1*, 76−87.


https://doi.org/10.1021/acsami.2c05952
*ACS Appl. Mater. Interfaces* XXXX, XXX, XXX−XXX